Macromolecules **2006,** *39,* 2330−2339

Polymer Chain Winding in the Melt

David G. Richardson[†] **and Cameron F. Abrams***

Department of Chemical and Biological Engineering, Drexel University, 3141 Chestnut St., Philadelphia, Pennsylvania 19104

Received September 12, 2005; Revised Manuscript Received January 3, 2006

ABSTRACT: We present the results of a series of molecular dynamics simulations of a melt of flexible bead−spring polymer chains with a single static cylindrical inclusion with diameter equal to the polymer beads. Chains of length $N = 10$, 25, 50, 100 and polymer/inclusion interactions, which are attractive with well depths of 1, 4, and 10 ϵ, and athermal, are considered. We show that the distribution in winding number of a polymer chain about the inclusion may be approximated by Belisle's probability distribution for the winding of a random walk about a point. The degree of winding per chain increases as the polymer/inclusion attraction increases because of the larger number of monomers pulled into runs of sequential monomers at the inclusion. Runs accumulate more winding than do loops or tails, and the amount of winding a given run accumulates increases with increasing polymer/inclusion attraction due to increased likelihood of perpendicular bond orientation with respect to the inclusion. The probability of winding depends on monomer distance from the inclusion in an apparently universal manner when distance is scaled by the unperturbed chain radius of gyration. Our results bear direct relevance to understanding the nature of enhancing toughness of polymeric materials by adding filler particles which increase the degree of entanglement.

I. Introduction

Dense systems of flexible polymers at concentrations above the so-called overlap threshold exist as entangled networks of chains.[1] Entanglements are thought of as topological features of the polymer network that in a broad sense restrict polymer chain motion. Although there is no consensus about the exact nature of entanglements, topologically speaking they must arise because chains can wind around one another. Intuitively, as the degree of winding increases between an entangled pair of chains, so too does the mutual restriction of each chain's motion, through a variety of topological and frictional mechanisms.

The work required to "disentangle" chains is thought to be largely responsible for the toughness of polymeric materials, primarily because polymeric solids craze significantly under tensile load prior to failure.[2] Toughness, among other material properties, can be enhanced by adding filler particles which, to an unknown extent, have the potential to increase the effective number of entanglements per unit volume. Fillers with nanoscopic dimensions for this and other reasons have received particular interest. High aspect-ratio nanoscopic filler particles, such as carbon nanotubes (CNTs),[3] when introduced into an entangled polymer melt, potentially provide targets about which the chains can wind, as depicted schematically in Figure 1. It is not clear to what extent winding about filler particles occurs in such systems or if putative enhancement in material strength could result from such winding increasing the number of entanglements per unit volume. Nevertheless, understanding winding and entanglements would be useful for polymer composite engineers concerned with controlling composite toughness.

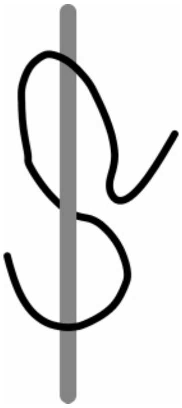

Figure 1. Schematic of a polymer chain (black) winding about a stiff cylindrical inclusion (gray).

There is some evidence that polymers wind about carbon nanotubes, which for several years have been suggested as the ultimate filler particle.[4−6] In TEM images, McCarthy and coworkers observed polymer deposition of periodic thickness on CNTs.[7] They conjectured that the periodic bundling observed in the TEM images is suggestive of many polymer chains winding around the CNT. Lordi and co-workers used atomically resolved energy minimization calculations to show that for certain polymers in a vacuum with a CNT the minimum-energy conformation occurs when the polymer chain is helically wound around the tube.[8] Although both of these works suggest the possibility of winding, neither offers any insight into the mechanism of wind formation nor the quality of chain winding in the melt. In fact, one should anticipate that because many more chains per unit volume interact with a filler particle in a melt than in more dilute solution, the nature of winding of chains in the melt is drastically different than in more dilute systems.

We use direct simulation of a simple model system to gain insights into the winding behavior of chains in the melt about stiff cylindrical inclusions, as a minimal model of nanotube-based polymer composites. Previous simulation research devoted to exploring the effects of polymer matrix/CNT interactions has focused on two areas: the load transfer abilities resulting from the formation of covalent bonds between the polymer matrix and the CNT inclusions[9−12] and the ability of CNTs to resist bending and deformation.[13−16] The effect of almost spherical

---

[†] Department of Computer Science, Drexel University, Philadelphia, PA 19104.

* Corresponding author. E-mail: cfa22@drexel.edu.

10.1021/ma051985d CCC: $33.50

nanoparticle inclusions in polymer melts has also been considered.[17−19] None of these works investigate polymer winding about the nanoparticle inclusions.

In this paper we focus on the propensity of generic polymer chains in a melt to wind about a cylindrical inclusion with aspect ratio akin to a CNT and of comparable diameter to the polymer persistence length. We have used molecular dynamics (MD) to generate equilibrium configurations of a generic bead−spring polymer melts with and without the inclusion. We have selected this generic model to allow the conditions under which winding may occur to be explored without reference to a specific atomistic system. This should provide a more direct view of the essential physics of winding. Additionally, it offers a significant reduction in the computational resources required to perform the simulations compared to an atomisticly resolved model. We consider chains of length $N = 10$, 25, 50, and 100. We consider inclusions that have no attractive interactions with monomers as well as inclusions of varying degrees of attractiveness.

The cylinders in our simulations (discussed in detail in the next section) are effectively inprenetrable, one-dimensional obstacles to the polymers. Much simulation work has previously been devoted to understanding polymer chain behavior near inpenetrable, two-dimensional walls (e.g., refs 20−22). We will discuss differences and similarities between these two cases in this paper; it is worth mentioning at the outset that our primary focus is on winding, which obviously cannot occur between a chain and a 2D surface.

Our findings may be summarized as follows. Chain ends are driven away from the inclusion when the polymer/inclusion interaction is strongly attractive. The random-walk scaling distribution of Belisle[23] is shown to predict the degree of winding remarkably well for the longest chains and weakest polymer/inclusion interactions. Because impenetrable obstacles can distort random walk statistics of melt chains,[21] this result was not guaranteed by the general propensity of polymer melts to be described by random walk. The average winding number of a chain appears to depend universally upon its distance from the inclusion when the distance is scaled by the unperturbed chain radius of gyration. Runs of sequential monomers along the inclusion accumulate more winding per unit chain length than do loops or tails, and the degree of winding accumulated in a run increases with increasing polymer/inclusion interaction strength. These results hint at future directions in developing a theory that captures the mechanisms of toughness enhancement of polymeric materials with nanoscopic fillers.

II. Simulation Methods

A. Model. The prototypical system in this study is a dense melt of bead−spring chains in a cubic box with a static inclusion made of a linear array of spherical particles fixed and equally spaced along the z-direction at the center. The two types of particles are polymer monomers and inclusion particles, and all are treated as point masses. The interaction potentials and potential parameters for all pairs of monomer types are selected such that the monomers are spherically symmetric with a diameter of 1 σ. The inclusion particles are placed every 1 σ along the z-axis of the simulation domain and are held fixed during the simulation. Because of periodic boundary conditions, this represents an infinitely long and stiff cylindrical inclusion. Reduced units are used throughout. ϵ is the base unit for energy, σ is the base unit for length, $m = 1$ is the base unit for mass, and $\tau = \sigma\sqrt{m/\epsilon}$ is the base unit for time.

Straightforward molecular dynamics (MD) simulation is employed to generate equilibrated melt configurations. MD numerically solves Newton's equations of motion for each particle, and particles interact according to a potential energy function, U. We employ a set of potentials to model the polymer chains which are standard for dense bead−spring melts. The bonded interactions along the polymer chain were modeled via the finitely extensible nonlinear elastic (FENE) potential:[24]

$$U_{\mathrm{FENE}}(r_{ij}) = -\frac{1}{2}\epsilon a {R_0}^2 \ln\left[1 - \left(\frac{r_{ij}}{R_0}\right)^2\right] \tag{1}$$

where a is a parameter representing bond strength, R_0 is a parameter representing the equilibrium bond distance, and r_{ij} is the scalar distance between monomers j and i. We use standard parameters of $a = 30$ and $R_0 = 1.5$ which effectively render impossible the crossing of bonds.[24]

Monomer−monomer excluded volume is modeled via the fully repulsive or "athermal" Weeks−Chandler−Andersen (WCA) potential:[25]

$$U_{\mathrm{WCA}}(r_{ij}) = \begin{cases} 4\epsilon\left[\left(\frac{\sigma}{r_{ij}}\right)^{12} - \left(\frac{\sigma}{r_{ij}}\right)^{6} + \frac{1}{4}\right], & r_{ij} < 2^{1/6}\sigma \\ 0, & r_{ij} \geq 2^{1/6}\sigma \end{cases} \tag{2}$$

For one series of simulations of melts of various chain lengths, the interaction between monomers and inclusion particles was also taken as the WCA potential. For the rest of the simulations, the interaction between monomers and inclusion particles is made attractive to varying degrees using a standard truncated and shifted Lennard-Jones (LJ) potential with the well depth labeled b:

$$U_{LJ}(r_{ij}) = \begin{cases} 4b\epsilon\left[\left(\frac{\sigma}{r_{ij}}\right)^{12} - \left(\frac{\sigma}{r_{ij}}\right)^{6} - \left(\frac{\sigma}{2.5}\right)^{12} + \left(\frac{\sigma}{2.5}\right)^{6}\right], & r_{ij} < 2.5\sigma \\ 0, & r_{ij} \geq 2.5\sigma \end{cases} \tag{3}$$

In addition to the athermal inclusion, we consider attractive inclusions with $b = 1$, 4, and 10. For each level of inclusion attractiveness, a single melt simulation is performed for each chain length, $N = 10$, 25, 50, and 100. Several melts with no inclusion are also considered for purposes of comparison.

The system is evolved through time using the velocity-Verlet leapfrog integrator[26] with a time step of 0.01. Only polymer monomers are allowed to move during the simulation. All simulations are conducted in the NVT ensemble using a Langvin thermostat[24] with a friction of 0.5 and a set-point temperature of 1.0. Particle pairwise interactions are identified using the combined neighbor list and the cell list method.[27]

B. Sample Preparation and Equilibration. For each simulation, M polymer chains of length N are randomly placed in the simulation domain. The size of the domain and number of chains are chosen such that (a) the total monomer number density including monomers from the inclusion is 0.85 and (b) the box dimension is integral and at least 4 times larger than the expected bulk radius of gyration of chains of length N. Bonded monomers are placed with an initial separation of the equilibrium FENE bond distance (i.e., the magnitude of separation where the FENE potential is at is minimum value). Each monomer is assigned a random velocity where each component was drawn from an exponential distribution with mean 1.0. Inclusions were evenly spaced along the z-axis of the simulation domain with unit separation between adjacent monomers.

This initialization procedure results in significant particle overlaps. To remove these overlaps, the simulations are "warmed up" with 2000 steps during which the nonbonded monomer monomer interactions were described by a radially shifted potential to reduce the forces to magnitudes that could be simulated without loss of stability. The strength of the magnitude of the radial shifting was linearly decreased each time step until at the end of the warm the nonbonded monomer−monomer interactions had reached full strength.[28] During the warm-up, velocities were rescaled and shifted so the average per particle kinetic energy was 1.0 and there was no center of mass velocity drift. After the warm-up, the equilibration phase of the simulation begins.

The equilibration time, τ_e, is defined as the time required on average for chains to diffuse a distance equal to their own radii of gyration. This was assessed by monitoring mean-squared displacements of monomers and chains. Data production begins after a few τ_e have elapsed from the warmed-up state.

C. Observable Definitions. Most observables have standard definitions, which for completeness we present briefly here. The mean-squared displacement for monomers, monomers relative to chain centers of mass, and centers of mass are denoted respectively g_1, g_2, and g_3, with the following definitions:

$$g_1(t) = \frac{1}{N}\sum_{i=1}^{N}\langle[\mathbf{r}_i(t) - \mathbf{r}_i(0)]^2\rangle \tag{4}$$

$$g_2(t) = \frac{1}{N}\sum_{i=1}^{N}\langle[\mathbf{r}_i(t) - \mathbf{r}_i(0) - \mathbf{r}_{cm}(t) + \mathbf{r}_{cm}(0)]^2\rangle \tag{5}$$

$$g_3(t) = \langle[\mathbf{r}_{cm}(t) - \mathbf{r}_{cm}(0)]^2\rangle \tag{6}$$

where $\mathbf{r}_i(t)$ is the position of monomer i at time t, $\mathbf{r}_{cm}(t)$ is the position of the chain center of mass at time t, and $\langle\ \rangle$ denotes an average over all chains and over all possible time origins.

The real-valued winding number of a chain, W, is defined as the number of times the chain winds around the z-axis:

$$W = \left|\frac{1}{2\pi}\sum_{i=2}^{N}(\phi_i - \phi_{i-1})\right| \tag{7}$$

where ϕ_i is the "x-convention" Euler angle ϕ used in specifying the position of monomer i. Winding angles are accumulated for each chain and subchain in the melt. W is a measurement associated with a single chain and a single inclusion. Because of the periodic boundary conditions, there is effectively an infinite array of inclusion images. We consider W to correspond to the winding of a chain about the image of the inclusion to which its center-of-mass is closest; i.e., the central image of the inclusion. Therefore, prior to analysis a chain's coordinates are unfolded, the chain center of mass is computed, and then folded into the primary box. The chain monomers are shifted by the same vector by which the center of mass is shifted.

We compute several quantities as functions of radial distance from the inclusion. For chain-specific properties, there are at least two ways to define the "distance" of a chain to the inclusion: (1) distance of the chain center of mass or (2) average monomer distance. Because chains can wind about the inclusion, it is often the case that chain centers of mass overlap the inclusion. For this reason, we have chosen to use the average monomer distance when discussing chain distance from the inclusion.

To investigate the influence of the inclusion on the distribution of chain ends as a function of distance from the inclusion, r, we define a chain end stoichiometric ratio profile

$$\alpha(r) = \frac{n_e(r)/n_i(r)}{2/(N-2)} \tag{8}$$

where $n_e(r)$ and $n_i(r)$ are respectively the number of chain end monomers and interior monomers at a distance r from the inclusion. The quantity $2/(N - 2)$ is the stoichiometric ratio of chain ends to chain internal monomers.

To investigate the shape and orientation of the polymer chains, we use the gyration tensor and second Legendre polynomial. The gyration tensor Q of a polymer chain is defined as having elements

$$Q_{\alpha\beta} = \frac{1}{N}\sum_{i=1}^{N}(r_{i,\alpha} - r_{cm,\alpha})(r_{i,\beta} - r_{cm,\beta}) \tag{9}$$

where $\alpha, \beta \in \{x, y, z\}$. The eigenvectors of Q correspond to the principal semiaxis and two minor semiaxes of an ellipsoid defining the average orientation of the polymer chain. The eigenvalues are the squared lengths of these axes, providing an approximate shape and size of the chain. The squared radius of gyration of a polymer chain is defined as

$$R_g^{\ 2} = \frac{1}{2N^2}\sum_{i=0}^{N}\sum_{j=0}^{N}(\mathbf{r}_i - \mathbf{r}_j)^2 \tag{10}$$

Note that R_g^2 is also the trace of the gyration tensor, Q. We compute R_g^2 in cylindrical coordinates to allow it to be easily resolved into components.

Each chain in a configuration contributes an orientation vector from the major axis of its Q which makes an angle θ with the global z-axis. A standard way to average over a field of vector orientations is to use the second Legendre polynomial with argument $\langle\cos\theta\rangle$. We compute the orientation profile as a function of average monomer distance, r, from the z-axis as

$$P_2^{\text{chain}}(r) = \frac{3}{2}\langle\cos^2\theta(r)\rangle - \frac{1}{2} \tag{11}$$

Note that $P_2(\theta) = -1/2$ indicates the vector field in the vicinity of r on average is perpendicular to the z-axis, $P_2(\theta) = 1$ indicates the field is parallel to the z-axis, and $P_2(\theta) = 0$ indicates the field is on average not oriented with respect to the z-axis. An analogous function, $P_2^{\text{bond}}(r)$, is used to asses the orientation of the vector field determined by individual bond orientations; in this case, r is the radial distance from the bond center to the inclusion.

We compute monomer density profiles as a function of distance from the inclusion. Monomers within a distance of 1.5 from the inclusion are considered to be in the first adsorbed shell. With this definition, we can partition all monomers in chains with at least one monomer in the first adsorbed shell as belonging to one of a run, loop, or tail. A run is a segment of consecutive monomers all contained in the first adsorbed shell. A tail is a segment of consecutive monomers that are not in the first adsorbed shell, but for which one end is a chain end and the other is bonded to the terminal monomer of a run. A loop is a consecutive segment of monomers such that none of the monomers are in the first absorbed shell and each end is bonded to a terminal monomer of a run.

III. Results and Discussion

A. Single Chain Dynamics: Assessment of Equilibration and Anisotropy of Motion. A summary of runs performed and their required equilibration times, τ_e, is provided in Table 1.

Table 1. Summary of Simulations Performed[a]

N	M	N_t	b	τ_e (τ)	D_z/D_{xy}	$D(\sigma^2/\tau)$
10	61	0	WCA	500	1.02	2.81×10^{-2}*
10	61	9	WCA	500	1.35	2.27×10^{-2}
10	61	9	1	500	0.98	2.77×10^{-2}
10	61	9	4	500	1.18	2.19×10^{-2}
10	61	9	10	500	1.31	1.69×10^{-2}
25	58	0	WCA	1000	1.34	9.56×10^{-3}
25	58	12	WCA	1000	1.16	8.52×10^{-3}
25	58	12	1	1000	0.84	6.57×10^{-3}
25	58	12	4	1000	1.18	7.35×10^{-3}
25	58	12	10	1000	1.07	5.87×10^{-3}
50	57	0	WCA	3500	1.25	3.76×10^{-3}
50	57	15	WCA	4000	0.95	2.83×10^{-3}
50	57	15	1	3500	1.29	3.35×10^{-3}
50	57	15	4	4000	1.25	2.95×10^{-3}
50	57	15	10	4000	0.98	2.07×10^{-3}
100	103	0	WCA	19500	0.95	1.11×10^{-3}
100	103	23	WCA	23500	1.08	9.23×10^{-4}
100	103	23	1	20500	0.99	9.73×10^{-4}
100	103	23	4	22000	1.03	9.51×10^{-4}
100	103	23	10	24000	1.17	1.01×10^{-3}

[a] Data are chain length (N); number of chains (M); length of inclusion/box size (N_t); polymer/inclusion interaction well depth (b) for which "WCA" signifies athermal; equilibration time (τ_e); ratio of diffusion constant in z vs in xy (D_z/D_{xy}); and the overall diffusion constant (D). $N_t = 0$ signifies a run with no inclusion. The data with an asterisk ($N = 10$ with no inclusion) is an average over 10 independent runs.

Equilibration times were estimated from the crossing of g_2 and g_3. The longest τ_e, about 2×10^4, was observed for $N = 100$. All simulations were conducted for a duration of 250 000, offering a reasonably large number of statistically independent configurations for use in calculating observables. We also observe that the degree of attraction between polymer and inclusion has little influence over τ_e.

The inclusion influences the dynamics of the melt in an anisotropic fashion to a marginal degree. We computed the ratio of the parallel to perpendicular (radial and tangential) diffusion constants, D_z/D_{xy}, according to

$$\frac{D_z}{D_{xy}} = \lim_{t\to\infty} \frac{2(g_3)_z}{(g_3)_x + (g_3)_y} \tag{12}$$

The overall diffusion constant is given by

$$D = \lim_{t\to\infty} \frac{g_3}{6t} \tag{13}$$

D and D_z/D_{xy} for each case considered appear in Table 1. We observe a slight anisotropy in the diffusive motion of chain centers of mass, averaging to about $\langle D_z/D_{xy}\rangle = 1.1$ over all runs with inclusions. (Ten independent runs of $N = 10$ with no inclusion showed an average D_z/D_{xy} of 1.02.) Generally speaking, then, motion parallel to the inclusion (i.e., in z) appears marginally faster than motion perpendicular to the inclusion, though this effect is rather weak and scattered. This anisotropy in D trends weakly from being a strong effect for short chains to a negligible effect for long chains, a result which at first blush might seem counterintuitive, given that long chains might entangle with the inclusion. We suggest that perhaps entanglements with the inclusion may form in the case of long chains are no more important in slowing the chains' diffusion that are entanglements with other chains. Nonetheless, a more precise analysis of the anisotropy of D would require better statistics, which we defer to a later study.

B. Liquid Structure. *1. Radial Density Distributions.* In Figure 2a, we plot the monomer number density, $\rho(r)$, as a function of radial distance, r, from the inclusion for chains of length $N = 100$ and for various levels of polymer/inclusion interaction strength. (Data for the shorter chain lengths are not significantly different and are therefore not shown.) Short-range decaying oscillations in density ranging out to about a distance of 4 from the inclusion are apparent, and this stratification becomes more pronounced as the inclusion becomes more attractive. Such density oscillations are typical of dense polymeric systems next to impenetrable obstacles, including flat walls (e.g., 20). Careful inspection of the data for $r < 1.5$ reveals that the total number of monomers in runs increases with well depth b.

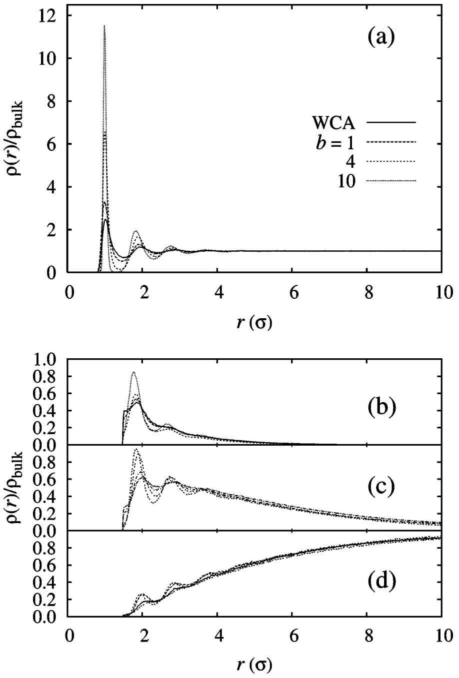

Figure 2. (a) Monomer density (normalized by the overall density, $\rho_{\mathrm{bulk}} = 0.85$) vs radial distance from inclusion, $\rho(r)$, for chain length $N = 100$ and various values of the polymer/inclusion interaction strength. Remaining panels show monomer density broken into monomers belonging to (b) loops, (c) tails, and (d) free chains.

Beyond a distance $r = 1.5$ from the inclusion, the liquid is composed of monomers belonging to (i) loops, (ii) tails, or (iii) chains with no monomer located less than $r = 1.5$, by definition. In Figure 2b−d, we plot monomer density as a function of r broken into these three categories, for chain length 100 and various levels of the polymer/inclusion interactions strength. The major interesting result in this figure is that the depth of penetration of loops and tails into the liquid does not depend on how strongly the inclusion attracts polymer. Making the inclusion more attractive merely stratifies the density of loop and tail monomers out to about $r = 4$. This is an important consideration because it means that the propensity of chains in the melt to bridge two inclusions should not depend on how attractive those inclusions are to the polymer. Moreover, because tails penetrate remarkably far into the liquid compared to loops, tails are more likely to bridge to other inclusions (assuming a uniform concentration of inclusions) in a multiinclusion system. The presence of long tails on chains partially adsorbed onto *flat* surfaces was first clearly explained by Scheutjens and Fleer using numerical self-consistent-field theory.[29] It is indeed interesting that this phenomenon arises about essentially line obstacles as well. Although there have been some theoretical calculations involving chains interacting with cylindrical particles (e.g., refs 30 and 31), we are unaware of such work meant to capture loop and tail length density distributions in the melt.

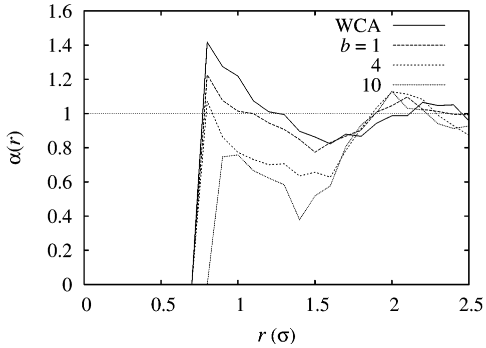

Figure 3. Chain-end stoichiometric ratio (eq 8) vs radial distance from inclusion, α(*r*), for chain length $N = 100$ and various values of the polymer/inclusion interaction strength.

Table 2. Summary of Structure of Single Chains and Liquid[a]

N	b	$\langle W \rangle$	$\langle l_{\text{run}} \rangle$	$\langle n_{\text{run}} \rangle$	$\langle l_{\text{loop}} \rangle$	$\langle n_{\text{loop}} \rangle$	$\langle l_{\text{tail}} \rangle$	$\langle n_{\text{tail}} \rangle$	$\langle P_2^{\text{bond}} \rangle$	$\langle \alpha \rangle$
10	WCA	0.15	2.15	1.19	2.14	1.40	2.98	1.49	0.018	1.08
10	1	0.16	2.41	1.17	2.04	1.38	2.80	1.47	0.023	0.98
10	4	0.17	2.84	1.14	1.88	1.33	2.58	1.46	−0.026	0.83
10	10	0.20	2.65	1.19	1.75	1.39	2.53	1.52	−0.108	0.51
25	WCA	0.22	2.34	1.69	3.77	1.97	7.79	1.70	0.015	1.12
25	1	0.22	2.65	1.58	3.73	1.86	7.71	1.69	0.018	0.98
25	4	0.24	3.18	1.54	3.54	1.81	7.31	1.72	−0.010	0.72
25	10	0.26	2.97	1.52	2.97	1.88	7.34	1.74	−0.058	0.46
50	WCA	0.27	2.36	2.19	5.92	2.50	16.12	1.81	0.008	1.10
50	1	0.27	2.72	2.11	6.07	2.43	15.73	1.80	0.011	0.97
50	4	0.33	3.23	1.98	6.02	2.23	15.52	1.83	−0.008	0.80
50	10	0.34	3.00	2.36	4.22	2.49	16.53	1.84	−0.037	0.46
100	WCA	0.28	2.41	2.52	8.82	2.71	29.56	1.89	0.003	1.09
100	1	0.27	2.72	2.47	9.31	2.67	28.84	1.88	0.007	0.97
100	4	0.31	3.31	2.29	8.80	2.52	28.78	1.91	−0.004	0.77
100	10	0.37	3.10	3.10	8.80	3.41	25.97	1.90	−0.023	0.53

[a] Mean winding number per chain, $\langle W \rangle$; mean run length, $\langle l_{\text{run}} \rangle$; mean number of runs per chain with at least one run, $\langle n_{\text{run}} \rangle$; analogous quantities for loops and tails; mean bond orientation index, $\langle P_2^{\text{bond}} \rangle$ averaged for bonds positioned less than 1.5 σ from the inclusion; and chain-end stoichiometric ratio averaged for monomers less than 1.5 σ from the inclusion, $\langle \alpha \rangle$.

Using both MC and MD, Daoulas et al.[22,33] considered a thin film of polyethylene confined between a vacuum and graphite sheet. The loop and tail density profiles observed by the wall are qualitatively different than those we observe by the tube. For the wall, the ratio of tail to loop monomers near the wall was almost 3. For the tube, this ratio was at most 1.5 for our longest chains. Given that the observations were for a generic tube and a wide range of attraction and chain length, it is unclear how this directly compares to the atomistically resolved system they studied.

The large penetration depth of tails leads one to expect that the stoichiometry of the melt (end monomers vs interior monomers) to be a locally variable function due to the inclusion. In Figure 3, we plot the chain-end stoichiometric ratio, α (eq 8), as a function of radial distance from the inclusion, for chains of length $N = 100$ for various levels of the polymer/inclusion interaction strength. Also included in Table 2 is the mean chain-end stoichiometric ratio, ⟨α⟩, averaged over chains with centers of mass between 0 and 1.5 σ from the inclusion, for all chain lengths and interaction strengths. We observe that increasing the attractive strength of the polymer/inclusion monomer interaction results in ends preferentially distributing themselves away from the inclusion. This is likely a result of the fact that the system enjoys an equivalent energetic advantage when an end or interior monomer interacts with the inclusion but pays a larger entropic penalty when an end monomer has its motion restricted by adsorption onto the inclusion.

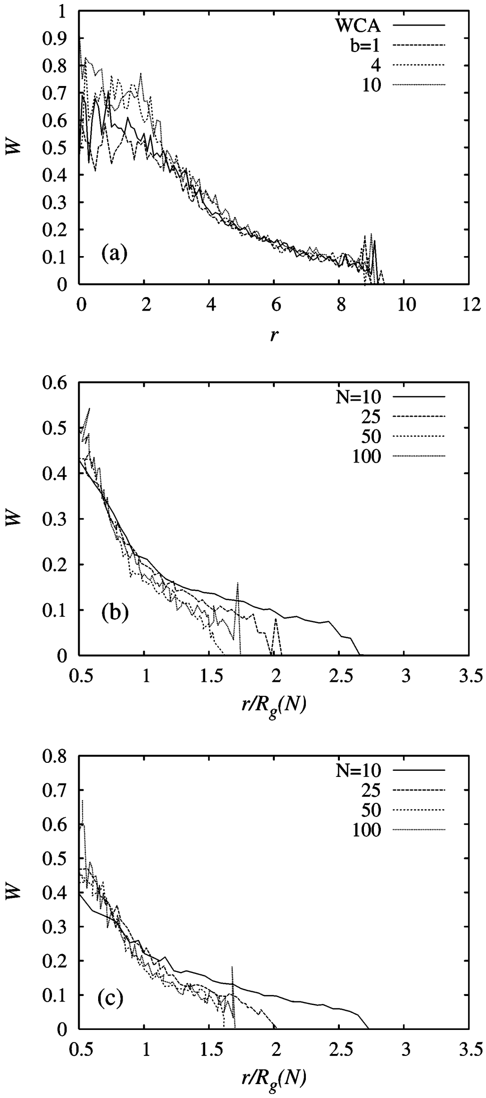

Figure 4. Winding number per chain, *W*, vs monomer radial distance from the inclusion for (a) $N = 100$ and various values of the polymer/inclusion interaction strength; (b) all chain lengths for the athermal polymer/inclusion interaction, with radial distance scaled by the respective bulk radius of gyration; and (c) all chain lengths for the attractive polymer/inclusion interaction with $b = 10$, also scaled as in (b).

End depletion has been observed in simulations of systems with flat walls. In similar coarse-grained MD simulations near a flat wall, Bitsanis et al.[20] observed an end enrichment near the wall that decreases as the wall−chain attractive interaction strength increases, similar to our findings with the cylindrical inclusion. Daoulas et al.[22,33] also observed an end depletion near the graphite wall.

Interestingly, as can be appreciated from the data in Table 2, placing end monomers further from the inclusion apparently does not result in an increased probability of *longer* tails; in fact, the opposite trend is observed. Both tails and loops sacrifice monomers to runs as the inclusion becomes more attractive. As the monomer density becomes more stratified, and end monomers are excluded from the first adsorbed shell, they experience difficulty approaching the inclusion on average any closer than about a distance of 2. This acts to decrease the fraction of chain ends below stoichiometric amounts close to the inclusion as the inclusion becomes more attractive.

2. Winding Number Profiles. In Figure 4a, we show representative profiles of the average winding number per chain as a function of average monomer radial distance from the inclusion, for athermal polymer/inclusion interactions. On average, the closer a chain places a monomer to the inclusion, the more it winds about the inclusion, and the longer the chain, the more it winds about the inclusion when it is a given distance away. When the radial distance is scaled by the respective R_g, as is shown in Figure 4b, we observe a nearly universal relation for $W(r)$ for all chain lengths considered, up to about $1.5R_g$. This appears reasonable as R_g defines the radius of the average volume in which a polymer chain is found. More interestingly, $W(r)$ decays relatively quickly with radius for $r < R_g$ and somewhat slows beyond this point, with the statistics becoming unreliable beyond about $r > 1.5R_g$. The quality of this universal agreement depends on the polymer/inclusion interaction strength, as we infer from Figure 4c, which shows $W(r)$ vs scaled r when the polymer is strongly attracted to the inclusion ($b = 10$).

This relationship could be of considerable practical importance for composite engineering. A universal dependence of chain winding number as a function of radial distance from an inclusion that scales in a predictable way with R_g would allow for calculation of the minimum filler particle density required for melt chains to wind around multiple filler particles simultaneously for any chain length. Intuitively, polymer networks where the average single chain entangles multiple filler particles would have an enhanced material toughness compared to polymer networks where the average single chain is entangled with fewer than two filler particles. (This hypothesis, however, should be tested.) If universal, this relationship offers the beginnings of a theory that can be used to provide a molecular foundation to explain the phenomenological observation that composite material properties vary with different filler particle densities.

C. Single Chain Structure. *1. Squared Radius of Gyration.* We report results regarding the effects of the inclusion on the structure of single chains and how they pack in the liquid. In Figure 5 we show profiles of R_g and its radial, tangential, and parallel components relative to the inclusion for athermal (Figure 5a−d) and attractive ($b = 10$; Figure 5e−h). Distance refers as usual to average monomer distance and is scaled by the respective bulk R_g in each case. First, we see that the inclusion weakly perturbs the components of R_g, stretching the chains in the direction of the inclusion and compressing them in directions normal to the inclusion. The level of attraction between the polymer and the tube has little influence.

While for a cylindrical inclusion there are two components perpendicular and one parallel, the reverse is true for a flat wall. From Bitsanis et al.,[20] we know that chains near a wall flatten in the direction normal to the wall and expand parallel to the wall, exactly analogously to the case with the cylinder. Similarly, it was also seen that, for all chain lengths and well-depths considered, the overall R_g varies by less that 10 from its bulk value.[20] With increasing the polymer/tube interaction strength, we observe almost no change in the tubes' influence on the R_g components. For the parameter values that Bitsanis explored, increased attractive strength resulted in a greater enlargement of the parallel component of R_g and a smaller reduction of the other components. As we have investigated a larger range of attraction than did Bitsanis, we conclude that a rod is less able to distort chain shape. In slight contrast, Daoulas et al.[22,33] observed that chain end-to-end distance increases normal to the wall and decreases parallel to it, though this was for a chemically specific polymer with one free surface and one solid surface.

2. Orientation Profiles. Given that the chain's shape is distorted by the inclusion, it is reasonable to ask if there is a preferred orientation the chains adopt relative to the inclusion. In Figure 6 we plot P_2^{chain} and P_2^{bond} (eq 11) as a function of distance from the inclusion for various chain lengths, again restricting the presentation to the illustrative cases of no attraction between polymer and inclusion and attraction with $b = 10$. (For P_2^{chain}, distance means perpendicular average monomer distance for a chain from the inclusion; for P_2^{bond}, distance means perpendicular center-of-bond distance from the inclusion.) There is a weak preferential perpendicular orientation caused by the inclusion. Increasing attractive strength results in an increase in the strength of the preferential orientation. In all cases, the chains whose orientation is most strongly affected by the inclusion are the shortest, $N = 10$. Because of their short length, these chains are more susceptible than are longer chains to sphere packing artifacts that occur because the inclusion and polymer monomers are composed of spherical particles. Nevertheless, chain orientation due to the inclusion is essentially negligible.

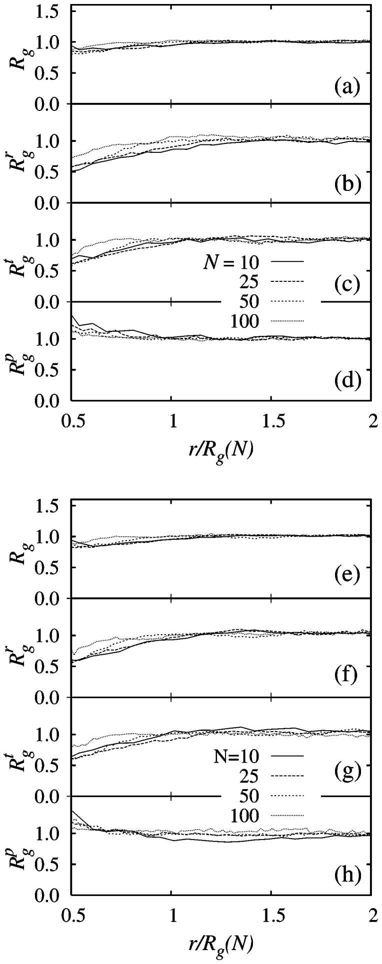

Figure 5. Radius of gyration and its components in cylindrical coordinates vs average monomer distance from inclusion, for various chain lengths, N. All data normalized to bulk values. Data for (a−d) athermal and (e−h) $b = 10$ are shown. Total R_g is shown in (a) and (e), radial component, R_g^r, is shown in (b) and (f); tangential, R_g^t, in (c) and (g); and parallel, R_g^p, in (d) and (h).

For P_2^{bond} (Figure 6b,d), we can see that increasing the well depth of the attractive potential results in the bonds having a slight favoring toward an orientation perpendicular to the tube. A perfectly perpendicular orientation minimizes the distance between each monomer and the tube, thus minimizing potential energy. Though this effect is rather weak in our system, it plays

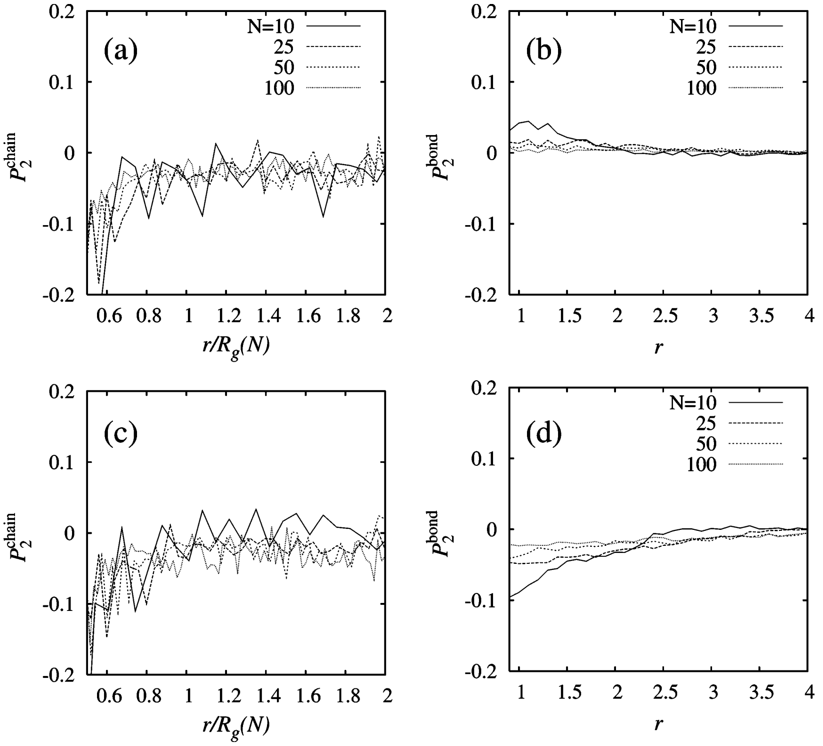

Figure 6. Chain and bond orientation indices, P_2^{chain} and P_2^{bond}, for various chain lengths, N, vs distance from inclusion. Data for (a, b) athermal and (c, d) $b = 10$ are shown. Distance for chain orientation index profiles is scaled by the respective bulk gyration radii.

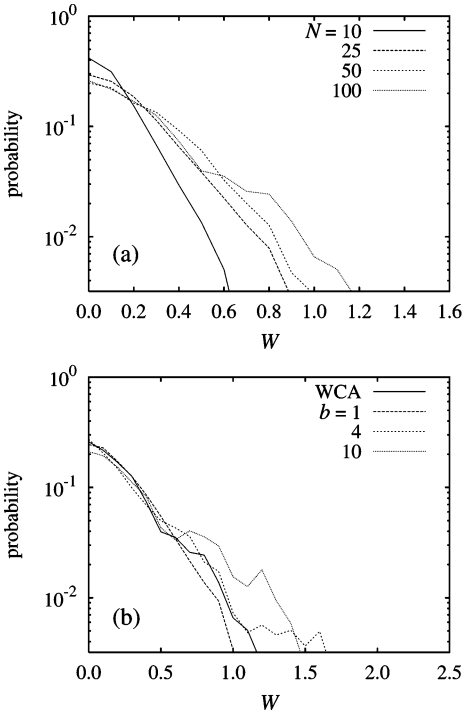

Figure 7. Representative probability distributions for winding number of chains around the cylindrical inclusion, W, for (a) all chain lengths N and athermal polymer/inclusion interactions and (b) chain length $N = 100$ and all polymer/inclusion interaction strengths.

an important role in explaining the nature of chain winding about the inclusion, as will be discussed in section III.C.4.

3. Winding Number Distributions. In Figure 7 we show several representative probability distributions of winding number per chain W (eq 7). These distributions are built by sampling all chains in each respective melt configuration. From Figure 7a, in which we consider all chain lengths ($N = 10$, 25, 50, and 100) for the case of athermal polymer/inclusion interactions, we see that longer chains have broader distributions in W. The means of all distributions of W, $\langle W \rangle$, are reported in column 3 of Table 2. The degree of winding per chain increases with chain length and generally increases with increasing attractiveness between monomers and the inclusion. This latter fact is illustrated in more detail in Figure 7b, in which we consider chains of length $N = 100$ for various degrees of attraction between polymer and inclusion. Here, higher winding numbers are more likely the more strongly attractive is the polymer/inclusion interaction.

To our knowledge, there is not yet a theoretical understanding of how the distribution in winding number depends on chain length or chain/inclusion interactions in the case of a dense melt. However, a melt chain configuration near a thin cylindrical inclusion can be represented as a 2D random walk in a plane to which the axis of the inclusion is orthogonal. Belisle[23] proved that for a random walker in the plane with finite step size that a scaling variable x measuring the degree of winding of the walk about the origin obeyed the following distribution:

$$\lim_{x\to\infty} P\left(x = \frac{2\theta}{\ln t}\right) = \frac{1}{2}\frac{1}{\cosh x} \tag{14}$$

where t is the number of steps taken by the walk and θ is the winding angle the walk makes about the origin. By taking into account the diffusion characteristics of such a random walk, Drossel and Kardar showed the following distribution is obtained:[32]

$$\lim_{x\to\infty} P\left(x = \frac{2\theta}{\ln r(t)^2}\right) = \frac{1}{2}\frac{1}{\cosh x} \tag{15}$$

where t has been replaced by the squared Euclidean distance the walk has traveled in time t from its origin, $r(t)^2$. The random walk model proposed by Belisle has been found to give excellent agreement with enumerated lattice random walks for 40 orders of magnitude of probability.[32]

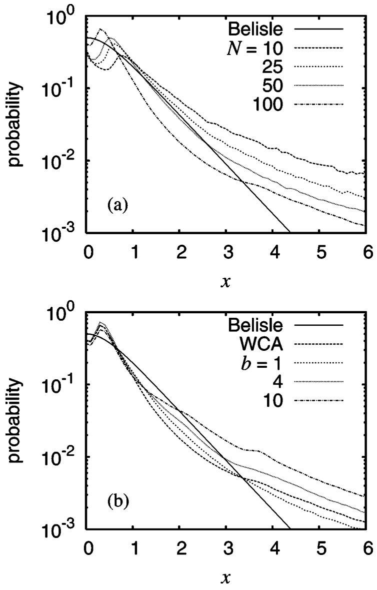

Figure 8. Representative probability distribution of the Belisle scaling variable, $x \equiv 2\theta/\ln(r(t)^2)$, for (a) no polymer/inclusion attraction for various chain lengths and (b) chain length $N = 100$ for various levels of polymer/inclusion interaction strength. The Belisle distribution is given in eq 15.

As chains in such melts are known to have random walk statistics,[24] we have investigated the ability of the Belisle distribution to describe winding of chains in the melt. In Figure 8 we plot the distribution of the Belisle scaling variable, x, extracted directly from our simulation configurations, together with the analytical expression in eq 15. We observe that without an attractive inclusion for chains of length $N = 100$ the Belisle distribution provides an remarkably accurate description for probabilities from 0.01 to 0.1 and values of the scaling variable from 1 to 3. As there are no parameters in the Belisle distribution, this favorable comparison is not the result of any fitting. This agreement provides evidence that, with respect to winding, the presence of the inclusion does not alter the random walk nature of the melt. This was not guaranteed, as Smith[21] has found that the random walk model cannot predict properties such as tail length near a flat wall.

When varying chain length, the Belisle distribution best describes the winding observed in the melt for longer chains. This is reasonable as the Belisle distribution applies strictly in the limiting case of infinitely long walks. When varying attractiveness, increased attractive strength results in successively worse agreement with the Belsile distribution. The presence of an attractive inclusion increases monomer density near the inclusion relative to a nonattractive inclusion (as will be discussed in detail in section III.B.1). As the Belisle distribution applies strictly for an unbiased walk, it is reasonable for the Belisle distribution have less success at predicting the behavior of chains with a preference for placing monomers near the inclusion.

There are several reasons for the limited range of agreement between the Belisle distribution and our simulation data. There are two ways the scaling variable may be less than unity: θ may be small or $r(t)^2$ may be large. Conversely, there are two ways the scaling variable may be large: θ may be large or $r(t)^2$ may be small. For short finite chains both θ and $r(t)^2$ must necessarily be small compared with what an infinitely long walk can achieve. This reduction in the range of values that θ and $r(t)^2$ may likely result in a biasing in the number of times different values of the scaling variable x are sampled relative to the case of an infinity long walk. As a result, these constraints placed on values of θ and $r(t)^2$ by the finite size of the chains are likely the cause of the deviations from the Belisle distribution at small and large values of the scaling variable. Additionally, we have on the order of 10 equilibration times of data from which to acquire statistics for the largest values of N. This is insufficient to observe events with a probability of occurrence much less than 10^{-3} with enough frequency for reliable statistics.

4. Run, Loop, and Tail Length Distributions. To gain a deeper understanding of how winding is structured in the melt, we consider how the chains partition their monomers into runs along the inclusion, loops with ends tethered at the inclusion, and tails with one end tethered and one end free. The mean lengths of runs, loops, and tails, $\langle l_{\mathrm{run}}\rangle$, $\langle l_{\mathrm{loop}}\rangle$, and $\langle l_{\mathrm{tail}}\rangle$, respectively, are reported in Table 2. The numbers of runs, loops, and tails per chain, $\langle n_{\mathrm{run}}\rangle$, $\langle n_{\mathrm{loop}}\rangle$, and $\langle n_{\mathrm{tail}}\rangle$, respectively, also appear in the table. The mean run length weakly increases with chain length for any level of polymer/inclusion interaction but displays a maximum with at $b = 4$ for all N. The lengths of loops and tails generally decrease as the inclusion becomes more attractive, signifying that, at least for moderate levels of attraction ($b < 10$), stronger attraction transfers more monomers from loops and tails into runs. Beyond moderate levels of attraction ($b > 4$), rather than strongly increasing the average run length, chains prefer to increase the number of runs. This results in a transition somewhere between $b = 4$ and 10 from fewer longer runs to a larger number of shorter runs with an overall increase in the number of adsorbed monomers.

The fact that tail lengths are all about $N/3$ echos the original findings of Scheutjens and Fleer in their self-consistent-field calculations of polymer solutions next to flat walls, when solvent volume fraction is small (i.e., melts).[29] As first pointed out by these authors, partially adsorbed chains project long tails into the liquid because many distinct chains compete for adsorption sites on the inclusion in systems with high polymer density. We observe that the average number of tails per chain is less than two for all chain lengths and interaction strengths and approaches two as chain length increases. This means that, per chain, shorter chains are more likely to adsorb an end than are longer chains.

The increase in average winding per chain considering only the athermal and $b = 10$ cases is mirrored by increases in similar relative magnitudes of the mean run length. However, $\langle W\rangle$ and $\langle l_{\mathrm{run}}\rangle$ are not directly proportional to one another for any b; were this the case, we would expect $\langle W\rangle$ to display a maximum for the intermediate $b = 4$, as does $\langle l_{\mathrm{run}}\rangle$. Even though the average run length decreases slightly moving from $b = 4$ to 10, the average winding per chain either stays the same or increases slightly. We suspect two major reasons for this behavior. Also shown in Table 2 is the mean orientational index of bonds between any two run monomers, denoted $\langle P_2^{\mathrm{bond}}\rangle$. As b increases, $\langle P_2^{\mathrm{bond}}\rangle$ trends more negative, indicating a weak preference for orienting bonds perpendicular to the inclusion axis. The more perpendicular a bond's orientation to the inclusion axis, the more winding it accumulates per unit length, making each run on average more efficient at winding. The second influence deals with the substantial increase in the average number of runs per chain, denoted $\langle n_{\mathrm{run}}\rangle$, and in the number of loops per chain, $\langle n_{\mathrm{loop}}\rangle$, as b moves from 4 to 10, especially for longer chain lengths. For $N > 50$, increasing the level of polymer/inclusion attraction beyond about $b = 4$, instead of resulting in longer runs, results in a larger number of runs and loops per chain.

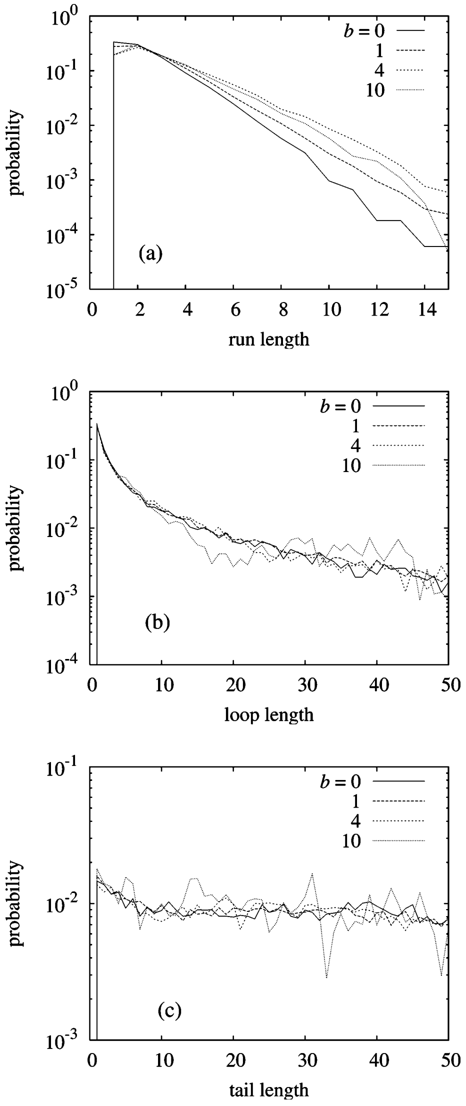

Figure 9. Distribution of length of (a) runs, (b) loops, and (c) tails for chain length $N = 100$ for various values of the polymer/inclusion interaction strength.

In considering the distributions in lengths of runs, loops, and tails, and how these are related to winding, we restrict our focus to chains of length $N = 100$. Distributions in lengths of runs, loops, and tails for $N = 100$ and various values of the polymer/inclusion interaction strength are shown in parts a, b, and c of Figure 9, respectively. There is little discernible influence of the well depth b on the length distributions of loops and tails. The run length distribution shifts to longer runs as b increases from 1 to 4 but then shifts again to shorter runs for $b = 10$. This reflects the increase in the number of runs and loops per chain as b moves from 4 to 10. The loop distribution does not appear to change much because the lengths of new loops as b increases are close to the peak value of about 1 or 2.

Smith et al.[21] used MD to investigate the behavior of FENE chains near both repulsive and attractive LJ walls. For chains of lengths between 20 and 100, run ("train") lengths of about three monomers are observed,[21] quite similar to what we observe here for chains near cylinders. The dimensionality of an inpenetrable obstacle appears to have little influence on the length of runs.

For each chain, we analyze how its overall degree of winding around the inclusion is distributed over runs, loops, and tails. In Figure 10, we plot the average winding number per run, loop, or tail respectively in parts a, b, and c as functions of length of run, loop, or tail. We observe that, of the three, runs contribute the most significant amount to winding and that the degree of winding is most sensitive to the length of runs compared to the lengths of loops or tails. The monomers near the inclusion are capable of accumulating a larger winding number per monomer because when close to the inclusion, the small displacements between bonded monomers have the potential to accumulate a larger winding angle. As increasing the attractive strength of the inclusion contracts monomers that would have been in loops and tails into runs, it appears that the primary mechanism by which an attractive inclusion introduces more winding is by bringing more monomers into runs and forcing bonds in runs to orient such that winding is more efficient. This is manifest as both an increase in run length at low to moderate levels of polymer/inclusion attraction and an increase in the number of runs per chains.

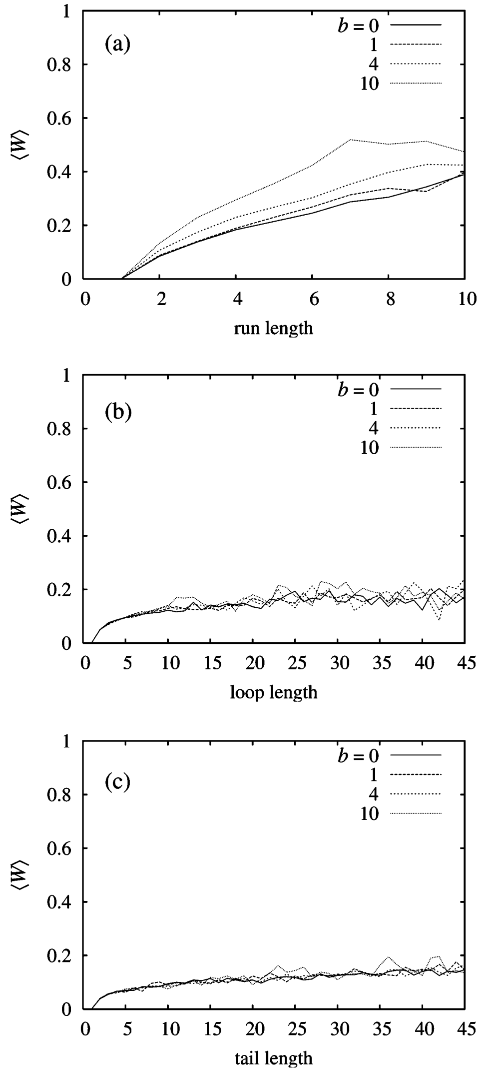

Figure 10. Average winding number per (a) run, (b) loop, and (c) tail for chain length $N = 100$ and for various values of the polymer/inclusion interaction strength.

The fact that monomers in runs accumulate more winding explains why end depletion near a tube does not decrease the average chain winding number. Any end monomer in the first adsorbed shell terminates a run. Removing an end from the vicinity of the inclusion offers the potential for longer runs and, consequently, higher average winding.

IV. Conclusions

We have conducted molecular dynamics simulations of dense bead−spring polymer melts with a single, rigid, immobile cylindrical inclusion. The presence of the cylindrical inclusion produces significant distortions in the structure of the polymer melt. As the attractive strength between the polymer and inclusion increases, the presence of the inclusion decreases the average size of chains near it, depletes the number of chain ends near the tube, and increases the amount of chain winding. Reminiscent of chains in the melt adsorbed to flat surfaces,[29] long tails penetrate quite deeply into the liquid. The inclusion introduces a minor preferred direction for polymer chain motion along the axis of the inclusion.

The most significant results of this work deal with the nature of winding of polymer chains about the inclusion. Despite its development for random walks that do not incorporate physical details such as excluded volume, bonds between monomers, or the fact that an attractive inclusion biases the chain walks toward the inclusion, the Belisle distribution[23] does reasonably well predicting winding angle distributions computed directly from melt simulation data and therefore could serve as the basis for a more chemically detailed theory of polymer chain winding. Moreover, we have found that the average winding number increases as inclusions are made more attractive to the polymer. For the chain lengths investigated, the winding angle profiles appear to be universally dependent upon the number of chain radii of gyration the monomer is away from the tube.

Taken together, these conclusions may indicate future directions for developing a theoretical understanding of nanocomposite toughness induced by control over entanglements. Future simulation studies must, however, be devoted to probing directly the toughness of a multiinclusion sample with the aim of understanding the degree to which undoing winds about the inclusions increases toughness. Such simulations are currently pursued by our group.

Acknowledgment. The authors are grateful to S. Obukhov for stimulating discussions. Financial support from the United States Office of Naval Research through Award N00014-03-1-0655 is gratefully acknowledged.

References and Notes

(1) de Gennes, P. G. *Scaling Concepts in Polymer Physics*; Cornell University Press: Ithaca, NY, 1979.
(2) Baljon, A. R. C.; Robbins, M. O. *Macromolecules* **2001**, *34*, 4200−4209.
(3) Iijima, S. *Nature (London)* **1991**, *354*, 56−58.
(4) Wanga, C.; Guob, Z.-X.; Fua, S.; Wub, W.; Zhu, D. *Prog. Polym. Sci.* **2004**, *29*, 1079−1141.
(5) Thostensona, E. T.; Ren, Z.; Chou, T.-W. *Compos. Sci. Technol.* **2001**, *61*, 1899−1912.
(6) Lau, K.-T.; Chipara, M.; Ling, H.-Y.; Hui, D. *Compos. Part B: Eng.* **2004**, *35*, 95−101.
(7) McCarthy, B.; Dalton, A. B.; Coleman, J. N.; Byrne, H. J.; Bernier, P.; Blau, W. J. *Chem. Phys. Lett.* **2001**, *250*, 27−32.
(8) Lordi, V.; Yao, N. *J. Mater. Res.* **2000**, *15*, 2770−2779.
(9) Frankland, S.; Harik, V.; Odegard, G.; Brenner, D.; Gates, T. *Compos. Sci. Technol.* **2003**, *63*, 1655−1661.
(10) Frankland, S.; Caglar, A.; Brenner, D.; Griebel, M. *J. Phys. Chem. B* **2002**, *106*, 3046−3048.
(11) Griebel, M.; Hamaekers, J. *Comput. Method. Appl. M* **2004**, *193*, 1773−1788.
(12) Gou, J.; Minaie, B.; Wang, B.; Liang, Z.; Zhang, C. *Comput. Mater. Sci.* **2004**, *31*, 225−236.
(13) Huhtala, M.; Kuronen, A.; Kaski, K. *Int. J. Mod. Phys. C* **2004**, *15*, 517−534.
(14) Shibutani, Y.; Ogata, S. *Model. Simul. Mater. Sci.* **2004**, *12*, 599−610.
(15) Fang, T.; Jian, S.; Chuu, D. *Chin. Phys. Lett.* **2004**, *21*, 1117−1119.
(16) Wei, C.; Cho, K.; Srivastava, D. *Phys. Rev. B* **2003**, *67*.
(17) Starr, F.; Schroder, T.; Glotzer, S. *Phys. Rev. E* **2001**, *64*.
(18) Starr, F.; Schroder, T.; Glotzer, S. *Macromolecules* **2002**, *35*, 4481−4492.
(19) Starr, F.; Douglas, J.; Glotzer, S. *J. Chem. Phys.* **2003**, *119*, 1777−1788.
(20) Bitsanis, I.; Hadziioannou, G. *J. Chem. Phys.* **1990**, *92*, 3827−3847.
(21) Smith, K. A.; Vladkov, M.; Barrat, J.-L. *Macromolecules* **2005**, *38*, 571−580.
(22) Daoulas, K. C.; Harmandaris, V. A.; Mavrantzas, V. G. *Macromolecules* **2005**, *38*, 5780−5795.
(23) Belisle, C. *Ann. Probab.* **1989**, *17*, 1377−1402.
(24) Kremer, K.; Grest, G. S. *J. Chem. Phys.* **1990**, *92*, 5057−5086.
(25) Weeks, J. D.; Chandler, D.; Andersen, H. C. *J. Chem. Phys.* **1971**, *54*, 5237−5247.
(26) Swope, W. C.; Andersen, H. C.; Berens, P. H.; Wilson, K. R. *J. Chem. Phys.* **1982**, *76*, 637−649.
(27) Frenkel, D.; Smit, B. *Understanding Molecular Simulation*, 2nd ed.; Academic Press: San Diego, 2001.
(28) Abrams, C. F.; Kremer, K. *J. Chem. Phys.* **2002**, *116*, 3162−3165.
(29) Scheutjens, J. M. H. M.; Fleer, G. J. *J. Phys. Chem.* **1980**, *84*, 178−190.
(30) Eisenriegler, E.; Hanke, A.; Dietrich, S. *Phys. Rev. E* **1996**, *54*, 1134−1152.
(31) Hanke, A. *J. Phys.: Condens. Matter* **2005**, *17*, S1731−S1746.
(32) Drossel, B.; Kardar, M. *Phys. Rev. E* **1996**, *53*, 5861−5871.
(33) Harmandaris, V. A.; Daoulas, K. C.; Mavrantzas, V. G. *Macromolecules* **2005**, *38*, 5796−5809.

MA051985D